

Characterize Then Distill: Mechanistic Reasoning in Large Output Spaces

Debjyoti Saha Roy, Byron C. Wallace & Javed A. Aslam
Khoury College of Computer Sciences, Northeastern University
{saharoy.d,b.wallace,j.aslam}@northeastern.edu

Abstract

Modern reasoning models offer surprisingly strong zero-shot performance on challenging multi-label tasks that require selecting a small set of relevant options from hundreds of thousands to millions of candidate labels. We investigate how they achieve this mechanistically. We characterize reasoning as a two-phase process: A broad “shortlisting” of candidates followed by fine-grained reasoning over the resulting set. We provide evidence across a range of datasets that these steps can be isolated and are complementary. Using this characterization, we develop a *mechanistic distillation* strategy that consistently outperforms standard distillation. We [open-source](#) code and trained models.

1 Introduction

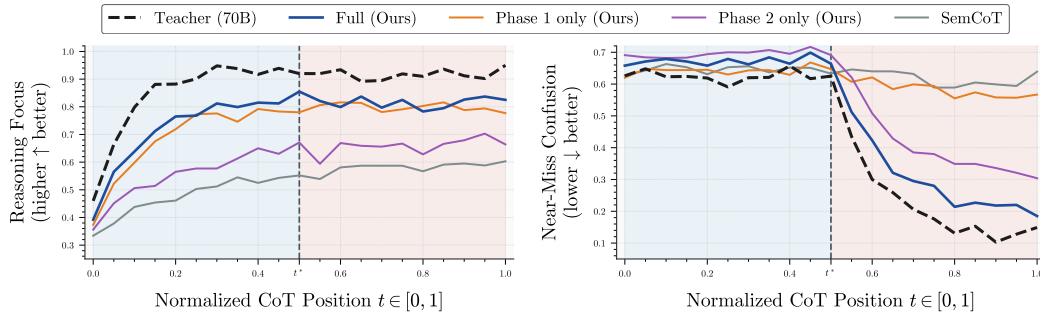


Figure 1: LLaMA3-70B exhibits early *Focus* buildup & late *Confusion* reduction over CoT. Mechanistic distillation recovers teacher trajectory while representative CoT distillations [He et al., 2025] fail.

In very large-scale multi-label settings, a small set of relevant labels must be selected from hundreds of thousands to millions of candidates [Zhou et al., 2024, Zhang et al., 2025, Ortego et al., 2025]. Such settings arise in applications like Wikipedia category tagging [Gupta et al., 2024, Dahiya et al., 2025], large-scale e-commerce categorization [Ortego et al., 2025], and document tagging in scientific repositories [Tabatabaei et al., 2025]. These kinds of tasks are challenging due to the prevalence of many rare “tail” labels with few examples.

This problem resembles the “needle-in-a-haystack” challenge in long-context evaluation, where models must retrieve or reason over sparse, critical information buried in vast distracting contexts [Kamradt, 2023, Hsieh et al., 2024]. This similarity suggests that challenging multi-label tasks may benefit from recent effective reasoning strategies that have succeeded for such problems. Recent reasoning models—such as OpenAI’s o-series [OpenAI, 2025a,b] and DeepSeek-R1 [Guo et al., 2025]—aim to emulate *System 2* reasoning [Zhang et al., 2024, Ji et al., 2025, Besta et al., 2025, Xu et al., 2025a, Li et al., 2025b]. Reasoning has enabled strong performance on long context tasks

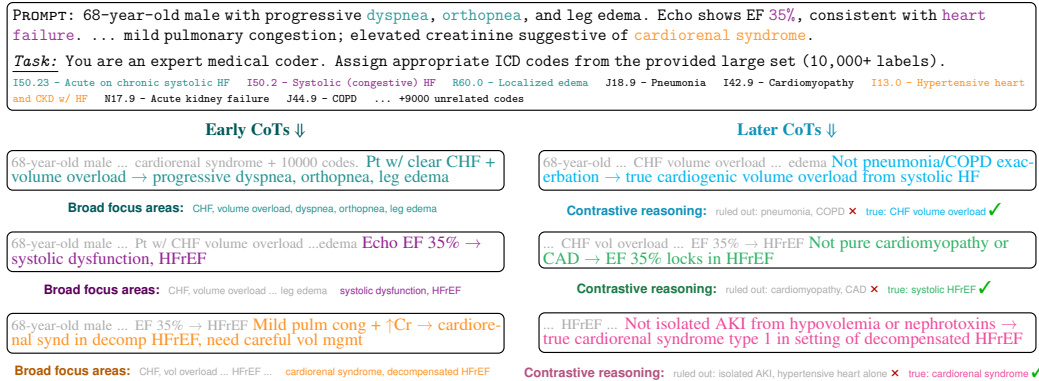


Figure 2: LLM Reasoning. (Left) Early CoT progressively builds focus on the broad categories. (Right) Late CoT progressively rules out near-miss categories until only the true signals remain.

[Modarressi et al., 2025, Wang, 2025, Kuratov et al., 2024, Marjanović et al., 2026], by leveraging structured mechanisms such as long Chain-of-Thought (CoT) [Chen et al., 2025a, Yeo et al., 2025], tree-of-thoughts [Yao et al., 2023], and deliberative reasoning [Guo et al., 2025, Guan et al., 2025].

We ask: **How do large reasoning models select a small set of relevant labels from millions of candidates without any task-specific training?** Past work on mechanistic interpretability [Bereska and Gavves, 2024, Hanna et al., 2024, Geiger et al., 2025, Du et al., 2025] has sought to characterize reasoning tasks like arithmetic [Nanda et al., 2023, Stolfo et al., 2023, Chen et al., 2025b], commonsense question answering [Chuang et al., 2025, Basu et al., 2025], ontology reasoning [Dutta et al., 2024], and code generation [Michaud et al., 2024]. But the mechanisms of reasoning over very large output spaces has not, to our knowledge, been explored.

We seek to characterize the implicit mechanisms used by large reasoning models and then systematically transfer them to smaller models. A simpler approach would be to use standard CoT distillation for this purpose, which has worked well for other tasks [Wang et al., 2023, Feng et al., 2024, Wadhwa et al., 2024, Chen et al., 2025c,d, Kang et al., 2025a, Li et al., 2025a]. These approaches aim to imitate the rationales from larger model rather than latent reasoning trajectories that give rise to them [Dai et al., 2024, Hu et al., 2026, Tan et al., 2026, Chen et al., 2026]. We observe that for these tasks smaller distilled models perform relatively poorly (35–38% drops in performance; Figure 1). We report that mechanistic distillation can result in stronger student model performance.

We evaluate performance along complementary dimensions for the teacher and its distilled student (formal definitions in Sec. 2): (1) **Reasoning focus** measures how early CoT aligns with the dominant semantic signal in the input, capturing progressive evidence consolidation into coherent anchors. (2) **Near-Miss Confusion** measures how strongly evolved reasoning remains aligned with plausible but incorrect alternatives, capturing the effectiveness of contrastive refinement in ruling them out.

As an illustration, consider the clinical example in Figure 2, which serves as a running example throughout the paper; the task is to assign the correct ICD¹ codes [WHO, 2025] from a large label space. An LLM exhibits *focused reasoning*: in early steps (left panel), it rapidly organizes evidence into coherent semantic anchors (e.g., grouping symptoms under heart failure, then refining to systolic dysfunction), effectively narrowing the search space. In later steps (right panel), it performs *contrastive refinement*, explicitly ruling out closely related alternatives (near-misses) such as competing diagnoses. This yields both high *focus* and low *confusion*. In contrast, smaller distilled models fail to maintain this structure: their reasoning drifts across loosely related concepts, lacking strong early anchoring and insufficiently separating true labels from plausible distractors.

Our **main contributions** are as follows: (1) We characterize and provide empirical, mechanistic evidence for a two-phase process in large reasoning models for challenging multi-label tasks—*coarse semantic filtering*, followed by *fine-grained reasoning over a small shortlist*—and show the phases are complementary and isolatable. (2) Using this characterization, we introduce a *mechanistic distillation* approach that directly supervises phase-specific computations at the level of aggregated attention heads and consistently outperforms standard CoT distillation.

¹Standardized medical labeling system with 10⁴–10⁵ codes, used as a benchmark for large-output tasks [Liu et al., 2023].

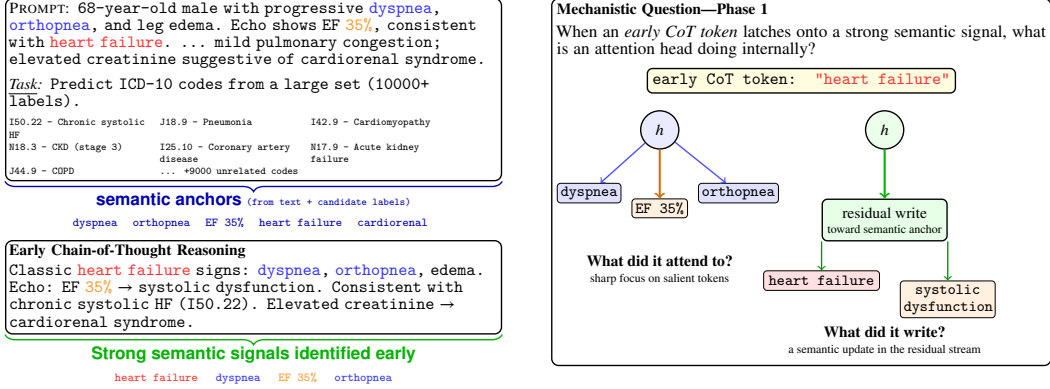


Figure 3: Phase 1—While generating early CoT, we measure whether attention heads attend to salient evidence and write semantically aligned updates as CoarseScore (Eq. 1).

2 How do Reasoning Models do Large-Scale Multi-Labeling?

We present a two-phase characterization of LLM reasoning in large spaces, with mechanistic evidence.

PHASE 1: COARSE SEMANTIC FILTERING

Figure 3 provides an example to build intuition for Phase 1. The *top-left panel* shows an input prompt and candidate label space, from which semantic anchors emerge. The *bottom-left panel* shows early CoT, where strong semantic signals (e.g., heart failure, EF 35%) are identified. The *right panel* poses the key question: *when these early CoT tokens are produced, what are the attention heads doing internally?* Specifically, do heads (i) focus on relevant evidence, and (ii) write updates aligned with the semantic signal? This setup generalizes to large output spaces tasks. Phase 1 captures this intuition via a *coarse score*, quantifying these properties, as detailed next.

Early-layer attention heads drive coarse filtering by linking salient input tokens to broad semantic anchors. To provide evidence for this, we construct prompts with controlled semantic signals and analyze attention patterns and head contributions during CoT via mechanistic interventions, motivated by prior work showing that a small subset of heads drives most long-context computation, while MLP layers play a limited role [Wu et al., 2024, Zheng et al., 2024, Tang et al., 2024, Fu et al., 2025]. We design *clean* prompts comprising text snippets with a strong coarse signal, followed by a long, multi-domain label list. For instance (Figure 3, *top left*), a heart failure discharge summary is paired with related ICD codes (cardiovascular/pulmonary) and unrelated domains. In turn, early CoT aligns with the dominant semantic signal in the input (i.e., cardiovascular concepts; *bottom left*).

For each head, we compute a *coarse filtering score* (Equation 1) on clean prompts, restricting the analysis to query positions from early CoT segments. Here $Q_{\text{early}}(x)$ denotes early-CoT query positions (first 10–30 generated tokens); α_q^h the attention distribution of head h at query position q , and; $\kappa(\alpha_q^h)$ its excess kurtosis, which identifies heads with sharply peaked attention patterns. $\Delta^h(q)$ denotes the residual-stream update written by head h at position q . Let $\mathcal{A}(x)$ be the set of relevant semantic anchors (e.g. cardiovascular conditions like “heart failure” or “pulmonary edema”) with embeddings $\mathbf{e}(y)$. Then the anchor centroid is defined as $\mathbf{c}_{\text{anchor}}(x) \triangleq \text{mean}_{y \in \mathcal{A}(x)} \mathbf{e}(y)$.

$$\text{CoarseScore}(h) = \mathbb{E}_x \left[\underbrace{\kappa(\alpha_{q,\cdot}^h)}_{\text{sharp attention (kurtosis)}} \cdot \underbrace{\cos(\Delta^h(q), \mathbf{c}_{\text{anchor}}(x))}_{\text{anchor-aligning write}} \right] \quad (1)$$

High CoarseScore values identify heads that **attend sharply to semantic anchors** and **align the residual representation with those anchors**. As illustrated in Figure 4 (*Left*), early-layer heads (e.g., L3H22, L2H7, and L1H12) in the LLaMA3–70B model dominate the top ranks during early CoT generation. Also, as illustrated in Figure 4 (*Right*), when a top-ranked early-layer head is queried from the position immediately preceding an early CoT token, its attention weights become sharply peaked on a small number of semantic anchors in the prompt, such as “heart failure”, “EF 35%”, and “prior

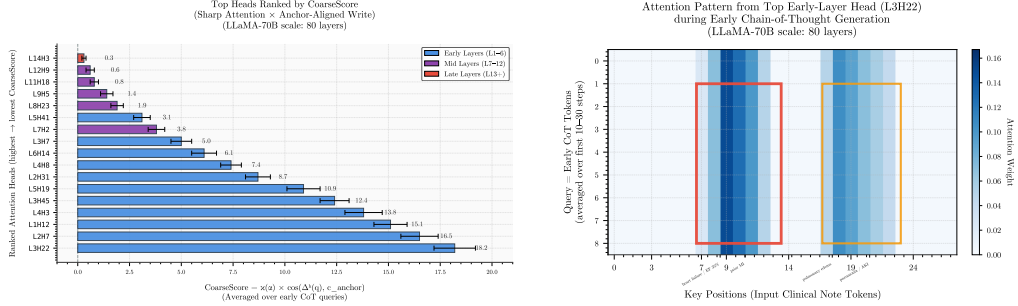


Figure 4: (Left) Top heads by CoarseScore in LLaMA3-70B model. Early-layer heads (L1–6) exhibiting anchor-focused attention and aligned residual updates during early CoT. (Right) Attention from a top early-layer head (L3H22), sharply focusing on key clinical anchors (red: cardiac phrases like “heart failure” and “EF 35%”; orange: respiratory/renal like “pulmonary edema” & “pneumonia”).

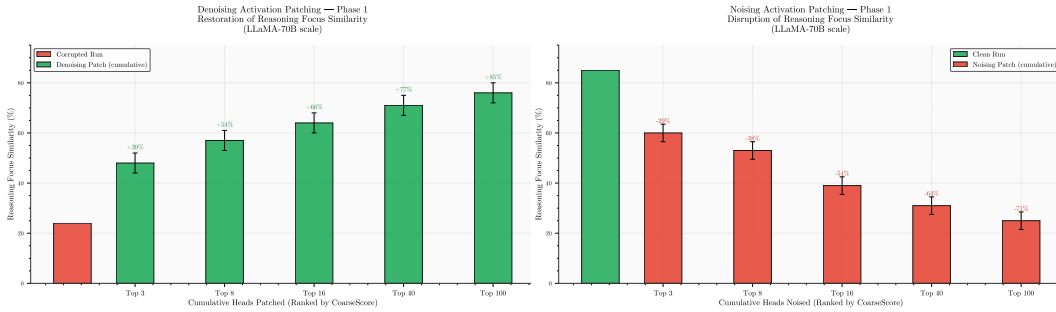


Figure 5: **Early-layer attention heads causally control coarse filtering.** (Left) Denoising patching progressively larger bins of top heads ranked by CoarseScore substantially restores reasoning focus toward semantic anchors. (Right) Noising these heads significantly degrades focus.

MI” (cardiac anchors), as well as related respiratory and renal anchors like “pulmonary edema” and “pneumonia”. This indicates early-layer heads rapidly detect and focus on relevant concepts. We then ask: *Do these peaked heads causally implement coarse filtering?*

To answer, we evaluated causal sufficiency/necessity using denoising/noising activation patching [Heimersheim and Nanda, 2024]. We ranked heads by CoarseScore (Equation 1) and grouped them into *cumulative bins* (Top 3, Top 8, Top 16, Top 40, Top 100). Within each bin, we patched the *attention patterns* of the selected heads, using randomly selected and low-ranked (count-matched) heads as negative controls. For patching, we *corrupted* the clean prompt by perturbing the text snippet to remove coarse semantic signal (e.g., replacing clinically meaningful terms like “dyspnea” or “heart failure” with neutral terms). Consequently, early CoT segments show weak alignment with the (original) input semantics. We measured a single metric capturing this alignment—*reasoning focus*—defined as how strongly early CoT tokens align with the dominant semantic signal in the clinical text portion of input x :
$$\text{Focus} = \mathbb{E}_{q \in \mathcal{Q}_{\text{early}}} \cos(e(r_q), \mathbf{c}_{\text{anchor}}(x)) \quad (2)$$
 where r_q denotes CoT token at position q (see Appendix B for details).

Figure 5 (Left) shows that denoising patching—replacing attention patterns in corrupted runs with those from clean runs—progressively restores reasoning focus toward cardiovascular semantic anchors in corrupted runs (up to 85% restoration). Even the top 3 heads provided meaningful recovery, with further gains as more heads were included, demonstrating *sufficiency*. Conversely, Figure 5 (Right) shows that noising these same heads in clean runs produced diffuse early CoT traces, significantly disrupting reasoning focus (up to 71% disruption), with noticeable degradation even for the top few heads and further collapse as more heads were noised, demonstrating *necessity*. In both cases the negative control heads defined earlier produced negligible effects. Together these results demonstrate that specific early-layer attention heads causally implement Phase 1 coarse filtering by linking salient tokens to broad semantic anchors, enabling early-stage pruning of the label space.

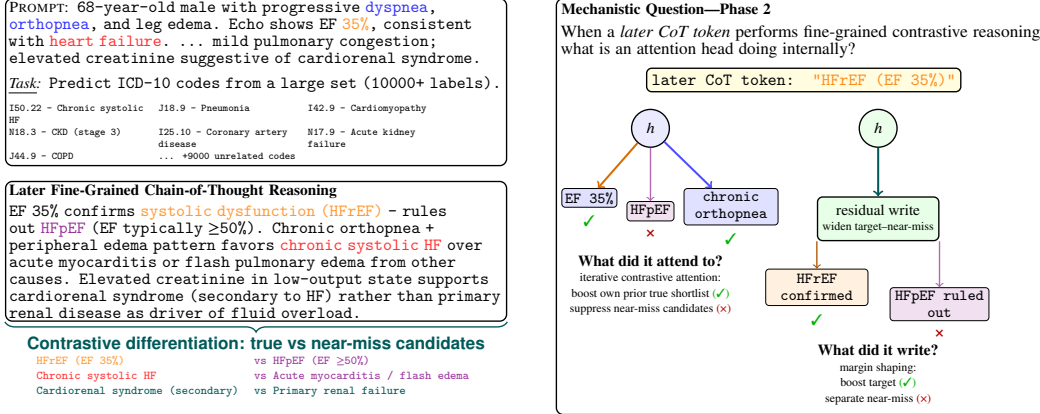


Figure 6: Phase 2—During later CoT, attention heads refine predictions by suppressing near-misses, widening margins between these and the correct labels (as captured by RefineScore; Equation 3).

PHASE 2: FINE-GRAINED REASONING OVER A SHORTLIST

Figure 6 conveys the intuition using the same representative example. The *bottom-left panel* shows later CoT, where the model contrastively differentiates among shortlisted candidates (e.g., HF_rEF vs. HF_pEF). The *right panel* asks: *When processing later CoT tokens, what are the attention heads doing internally?* We argue that they (i) iteratively attend to prior shortlisted candidates, reinforcing true ones while suppressing near-misses, and; (ii) write updates that widen the margin between target and competing alternatives. We quantify this intuition via a *refine score*, defined below.

Later-layer attention heads drive Phase 2 iterative refinement by re-attending to the model’s own earlier representations of the retained shortlist and widening margins between target and near-miss subcategories. To investigate and provide evidence we perform mechanistic interventions analogous to Phase 1. We first ask: *Which heads iteratively loop back to their own prior representations of the retained shortlist while suppressing representations of subcategories that were previously shortlisted but have since been ruled out (near-misses)?* To answer, for each head h , we define a QK -refinement score. We mark position q in the CoT as *refinement position* if it contains contrastive reasoning (like confirming “HF_rEF” and ruling out “HF_pEF” in the bottom-left cardiovascular example of Figure 6). At refinement positions q , we extract the head-specific query vector \mathbf{q}_q^h . For earlier positions p where the CoT explicitly referenced shortlist candidates (tokens like “HF_rEF/systolic”) or ruled out near-miss subcategories (“HF_pEF/diastolic”), we extract key vectors \mathbf{k}_p^h . We then compute $\text{Sim}_{\text{shortlist}}(q) = \mathbb{E}_{p \in S} \cos(\mathbf{q}_q^h, \mathbf{k}_p^h)$ and $\text{Sim}_{\text{near}}(q) = \mathbb{E}_{p \in \mathcal{N}} \cos(\mathbf{q}_q^h, \mathbf{k}_p^h)$, where S and \mathcal{N} denote shortlist and near-miss positions, respectively. Then we compute the refinement score as, $\mathbb{E}_q[\text{Sim}_{\text{shortlist}}(q) - \text{Sim}_{\text{near}}(q)]$ averaged over refinement positions and examples.

$$\text{RS}(h) = \mathbb{E}_{q \in \mathcal{R}(x)} \left[\underbrace{\left(\mathbb{E}_{p \in S(x)} \cos(\mathbf{q}_q^h, \mathbf{k}_p^h) - \mathbb{E}_{p \in \mathcal{N}(x)} \cos(\mathbf{q}_q^h, \mathbf{k}_p^h) \right)}_{\text{QK loop-back (where to read)}} \cdot \underbrace{\langle \Delta^h(q), \nabla_{\mathbf{h}_{\text{final}}(q)} \text{margin}(q) \rangle}_{\text{OV helpfulness (what to write)}} \right] \quad (3)$$

Do these heads also write residual updates that widen target–near-miss margins via OV? To investigate, we define a *OV-helpfulness* score per head. For each refinement position q we look at every position p (previous mention of shortlist token) that this head was paying significant attention ($\alpha > 0.3$). We call these position attended shortlist ‘keys’. Then we get the head updates for these ‘key’ positions using: $\Delta^h(q) = \sum_{\text{keys}} W_O^h(\alpha \cdot W_V^h \mathbf{h}_{\text{key}})$. To measure how strongly the model favors correct shortlist labels over the near-miss labels at refinement step q , we define $\text{margin}(q) = \text{avg_logit}_{\text{target}}(q) - \text{avg_logit}_{\text{near_miss}}(q)$ (see Appendix B, Equation 7). Then to measure how much an head update aligns in a direction that favors the target logits—for example, by increasing $\text{logit}(\text{systolic})$ relative to $\text{logit}(\text{diastolic})$ —we compute *OV-helpfulness* score as: $\text{OV}_{\text{help}}^h(q) = \Delta^h(q) \cdot (\partial \text{margin}(q) / \partial \mathbf{h}_{\text{final}}(q))$, averaged over refinement positions and examples. Finally, we compute RefineScore as the product of QK and OV scores (Equation 3).

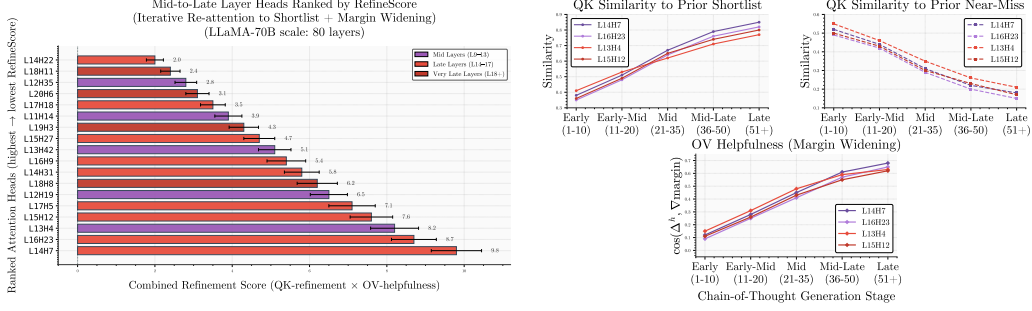


Figure 7: **Later-layer heads showing iterative refinement.** (Left) Mid-to-late attention heads ranked by QK preference for own prior shortlist keys over near-miss keys + OV updates widening margins. (Right) Over CoT, top refinement heads sharpen QK preference toward shortlist representations, downweight near-misses, and strengthen OV contributions for iterative margin widening.

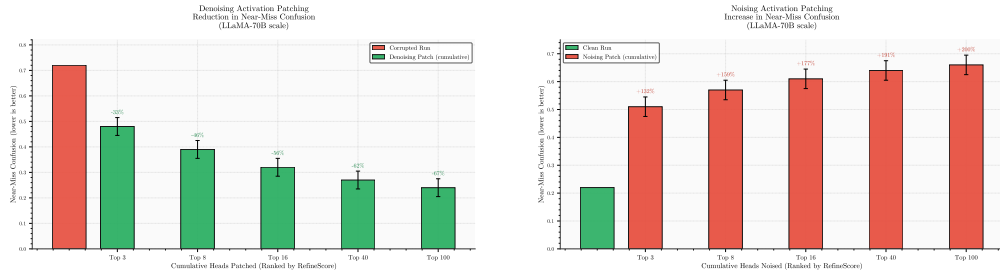


Figure 8: **Later-layer heads causally drive iterative refinement.** (Left/Right) Denoising successively larger bins of top RefineScore-ranked heads sharply $\downarrow\downarrow$ near-miss confusion & noising them $\uparrow\uparrow$ it.

High positive RefineScore identifies heads that re-attend to prior shortlist representations while avoiding near-misses, and write updates that widen the target–near-miss margin. As illustrated in Figure 7 (Left), mid-to-late heads (L14 and above) in LLaMA3–70B show strong iterative looping and discriminative updates. Figure 7 (right) illustrates the temporal dynamics of the top ranked heads across CoT stages (x-axis: Early to Late tokens). These heads show increasing QK similarity to their prior shortlist (top-left) while decreasing similarity to near-miss candidates (top-right), e.g., attending more to “EF 35% confirms systolic dysfunction (HF_rEF)” and less to “HF_pEF ($\geq 50\%$)” or “acute myocarditis” as the CoT progresses. Concurrently, the OV circuit (bottom) shows rising alignment ($\cos(\Delta^h, \nabla \text{margin})$) with widening the logit margin between correct and alternative options—“chronic systolic HF” vs. “flash edema”, and “secondary cardiorenal syndrome” vs. “primary renal disease”—supporting contrastive reasoning in later stages.

Finally, we ask: *Do these heads causally drive iterative refinement?* Similar to Phase 1, we perform activation patching: We ranked heads by *refinement score*, formed cumulative bins (Top 3–100), and patched their *attention patterns*, using count-matched random and low-ranked heads as controls. We corrupt the clean prompt by perturbing the text snippet to favor near-miss subcategories—for example, in the cardiovascular (top left panel) prompt in Figure 6, replacing progressive→acute, EF 35% → 55%, and cardiorenal syndrome → primary renal failure. Consequently, later CoT segments gets steered toward the near-miss semantics rather than the true target, e.g., toward diastolic interpretation as opposed to systolic for a clean prompt. We measure a single metric capturing this effect—*near-miss confusion*—defined as how strongly the *anchor-conditioned late*

CoT aligns with near-miss representations: $\text{Confusion} = \mathbb{E}_{q \in \mathcal{R}_{\text{refine}}} \cos(e(s_q), \mathbf{c}_{\text{near}}(x))$, (4) where $s_q = a(x) \parallel [r_1 \dots r_q]$ is the cumulative prefix formed by appending refinement CoT tokens to a fixed anchor text, and $\mathbf{c}_{\text{near}}(x)$ denotes the centroid of near-miss categories $\mathcal{N}(x)$ (see App. B for details).

Figure 8 (Left) shows that denoising patching progressively lowers near-miss confusion at refinement positions. Even the top 3 heads provided sharp reduction, with further improvements as more heads were included (upto 67% reduction with the top 100 heads), proving *sufficiency*. Conversely, noising the same heads (right panel) steers the refinement–CoT toward near-miss subcategories, boosting near-miss confusion by up to 200%, proving *necessity*. Negative controls had negligible effects in both cases. Together these results demonstrate that specific mid-to-late layer heads causally implement sharp distinctions between target and near-miss subcategories during contrastive reasoning.

3 How Can We Distill the Reasoning Mechanism?

Having characterized two mechanisms for large-scale multi-labeling—Phase 1 coarse filtering and Phase 2 iterative margin refinement—we perform *mechanistic distillation*. To align phase-specific signals, we distill via teacher forcing on the teacher-generated CoT trace [Wang et al., 2023, Yan et al., 2025, Chen et al., 2025d, Fang et al., 2026]. For input x , the teacher produces $\tau^T(x)$, and both models are run on $z^T(x) = [\text{prompt}(x); \tau^T(x)]$, allowing comparisons at aligned query positions. Our goal is to transfer not merely the teacher’s generated tokens, but the underlying *mechanics* that produce them. Our distillation objective mirrors this. Because teacher and student heads may not align one-to-one, we identify high-scoring head *pools* for each phase and distill three signals: (1) *where* the model reads, (2) *what* it writes into residual stream, & (3) the interaction between the two.

For Phase 1 we select the top- k early-layer heads by the coarse-filtering score (Eq. 1); for Phase 2 the top- k mid-to-late heads by the refinement score (Eq. 3). Let $\mathcal{H}_{\text{P1}}^{(T,S)}$ denote the resulting head sets. For $M \in \{T, S\}$ and $h \in \mathcal{H}_{\text{P1}}^M$, we assign normalized weights $w_h^M = \frac{\exp(\text{CS}^M(h)/\tau)}{\sum_{h'} \exp(\text{CS}^M(h')/\tau)}$, $h' \in \mathcal{H}_{\text{P1}}^M$, where τ controls weight sharpness. Phase 2 uses same weighting scheme, replacing CS with RS.

Phase 1 heads route attention toward salient tokens during early reasoning (cf. Eq. 1). To distill this behavior, we pool attention using the head sets and weights defined above: $\tilde{\alpha}_{q,\cdot}^M = \sum_h w_h^M \alpha_{q,\cdot}^{M,h}$, $h \in \mathcal{H}_{\text{P1}}^M$, $M \in \{T, S\}$. **Phase 1 heads also write updates that align the residual representation with the relevant semantic anchor** (cf. Eq. 1). To distill this behavior, we pool write vectors using the head sets and weights defined above: $\tilde{\Delta}^M(q) = \sum_h w_h^M \Delta^{M,h}(q)$, $h \in \mathcal{H}_{\text{P1}}^M$, $M \in \{T, S\}$. We then compute the anchor-alignment score $A^M(q) = \cos(\tilde{\Delta}^M(q), \mathbf{c}_{\text{anchor}}(x))$. **Phase 1 coarse filtering arises from the interaction between sharp attention and anchor-aligning writes** (cf. Eq. 1). To distill this joint behavior, we match a pooled coarse-filtering score combining pooled attention and pooled writes. For $M \in \{T, S\}$ we define $\text{PCS}^M(q) = \kappa(\tilde{\alpha}_{q,\cdot}^M) \cdot \cos(\tilde{\Delta}^M(q), \mathbf{c}_{\text{anchor}}(x))$, mirroring multiplicative structure of Eq. 1 at the pooled-head level (cf. App. B). *We minimize the teacher–student discrepancies in $\tilde{\alpha}_{q,\cdot}^M$, $A^M(q)$, and $\text{PCS}^M(q)$ via the KL, write, & interaction terms in Eq. 5.*

$$\begin{aligned} \mathcal{L}_{\text{attn}}^{\text{P1}} + \mathcal{L}_{\text{write}}^{\text{P1}} + \mathcal{L}_{\text{int}}^{\text{P1}} &= \mathbb{E}_x \left[\text{KL}(\tilde{\alpha}_{q,\cdot}^T, \tilde{\alpha}_{q,\cdot}^S) + (A^T(q) - A^S(q))^2 + (\text{PCS}^S(q) - \text{PCS}^T(q))^2 \right], \quad (5) \\ \mathcal{L}_{\text{loop}}^{\text{P2}} + \mathcal{L}_{\text{write}}^{\text{P2}} + \mathcal{L}_{\text{int}}^{\text{P2}} &= \mathbb{E}_x \left[(R^T(q) - R^S(q))^2 + (H^T(q) - H^S(q))^2 + (\text{PRS}^T(q) - \text{PRS}^S(q))^2 \right]. \quad (6) \end{aligned}$$

Phase 2 heads refine decisions by repeatedly re-attending to previously mentioned shortlist representations while suppressing near-miss alternatives (cf. Eq. 3). Phase 2 heads also write residual updates that widen the margin between target and near-miss labels via the *OV circuit* (cf. Eq. 3). **Phase 2 refinement emerges from the interaction between loop-back retrieval and margin-widening writes** (cf. Eq. 3). Analogous to the Phase 1 distillation outlined above, we distill pooled Phase 2 refinement heads using signals: (1) loop-back retrieval behavior, (2) margin-improving write updates, and (3) their interaction. Due to space constraints, we defer the full formulation and definitions of $R^M(q)$, $H^M(q)$, and $\text{PRS}^M(q)$ to App. B; the resulting objective is shown in Eq. 6.

The final objective combines standard CoT distillation with our mechanistic distillation: $\mathcal{L}_{\text{total}} = \underbrace{\mathcal{L}_{\text{CoT}}}_{\text{vanilla CoT distillation}} + \underbrace{\lambda_{\text{P1}} \mathcal{L}^{\text{P1}} + \lambda_{\text{P2}} \mathcal{L}^{\text{P2}}}_{\text{mechanistic distillation (ours)}}$ where \mathcal{L}_{CoT} is the standard token-level distillation loss

under teacher forcing (App. B), \mathcal{L}^{P1} and \mathcal{L}^{P2} are the Phase 1&2 mechanistic losses (Eqs. 5, 6), and $\lambda_{\text{P1}}, \lambda_{\text{P2}}$ weight the coarse-filtering and refinement supervision terms.

4 Do Mechanistically Distilled Students Reason Like the Teacher?

Setup & Baselines. We evaluate on MIMIC-IV-full (ICD-10 coding from ICU discharge summaries) and LF-WikiSeeAlso-320K (Wikipedia related-article recommendation), following recent work [Johnson et al., 2023, Dahiya et al., 2025]; cf. App. C for details. We use a LLaMA-70B teacher

Table 1: **Mechanistic distillation improves reasoning quality, downstream performance, and recovers phase-specific reasoning mechanisms** on the MIMIC-IV-full dataset. See Table 2 in the appendix for results on LF-WikiSeeAlso-320K. Results across both datasets and additional student models (GEMMA-3-12B, QWEN3-4B) are in App. F, Tables 3 and 4.

Model/Method	Foc \uparrow	Conf \downarrow	LAS \uparrow	F1 \uparrow	Sharp \uparrow	Align \uparrow	Loop \uparrow	Help \uparrow
LLaMA3-7B/Vanilla	0.39	0.35	0.69	0.42	1.62	0.38	0.27	0.24
LLaMA3-7B/UniCoTT	0.48	0.29	0.73	0.47	1.85	0.44	0.34	0.31
LLaMA3-7B/MoRSD	0.51	0.27	0.74	0.49	1.92	0.46	0.36	0.33
LLaMA3-7B/SemCoT	0.47	0.30	0.72	0.46	1.79	0.43	0.32	0.29
LLaMA3-7B/CWT	0.53	0.26	0.75	0.50	1.98	0.47	0.38	0.35
LLaMA3-7B/Mech.	0.62 ^{*(+0.09)}	0.19 ^{*(-0.07)}	0.76 ^{*(+0.01)}	0.52 ^{*(+0.02)}	2.18 ^{*(+0.20)}	0.55 ^{*(+0.08)}	0.46 ^{*(+0.08)}	0.41 ^{*(+0.06)}
LLaMA3-13B/Vanilla	0.45	0.31	0.72	0.48	1.75	0.43	0.31	0.28
LLaMA3-13B/UniCoTT	0.54	0.26	0.75	0.52	1.96	0.49	0.38	0.35
LLaMA3-13B/MoRSD	0.56	0.24	0.76	0.54	2.04	0.51	0.40	0.37
LLaMA3-13B/SemCoT	0.53	0.27	0.74	0.51	1.91	0.48	0.36	0.33
LLaMA3-13B/CWT	0.58	0.23	0.77	0.55	2.09	0.52	0.42	0.39
LLaMA3-13B/Mech.	0.66 ^{*(+0.08)}	0.17 ^{*(-0.06)}	0.78 ^{*(+0.01)}	0.57 ^{*(+0.02)}	2.28 ^{*(+0.19)}	0.59 ^{*(+0.07)}	0.50 ^{*(+0.08)}	0.44 ^{*(+0.05)}
Avg. gain with mech.	$\Delta+0.136$	$\nabla-0.098$	$\Delta+0.033$	$\Delta+0.051$	$\Delta+0.339$	$\Delta+0.109$	$\Delta+0.126$	$\Delta+0.101$
LLaMA3-70B/Teacher	0.73	0.14	0.83	0.64	2.45	0.65	0.57	0.52

and LLaMA-7B/13B students, trained under teacher forcing on identical teacher-generated CoT traces. Baselines use standard CoT distillation (token-level cross-entropy + KL; see App. B), as well as recent strong methods: (1) UniCoTT [Zhuang et al., 2025]: structural CoT distillation; (2) MoRSD [Yan et al., 2025]: self-guided rationale selection; (3) SemCoT [He et al., 2025]: implicit-token CoT; (4) CWT [Chen et al., 2025c]: chunk-wise CoT training. Our method augments standard CoT with phase-specific supervision (Eqs. 5, 6): $\mathcal{L}_{\text{CoT}} + \lambda_{P1}\mathcal{L}^{P1} + \lambda_{P2}\mathcal{L}^{P2}$. We tune λ_{P1} , λ_{P2} on validation and keep training budget and optimization fixed across methods. Inference uses greedy decoding (temperature = 0), generating full CoT traces followed by final multi-label predictions.

Evaluation Metrics. We evaluate distillation quality using CoT fidelity metric of teacher-faithfulness, measured by Leakage-Adjusted Simulatability (LAS; App. D.1) [Wang et al., 2023]. To assess whether student recovers the phase-specific mechanisms from Section 2, we measure: (a) **Reasoning Focus** which captures Phase 1 (coarse filtering; Eq. (2)), (b) **Near-Miss Confusion** which captures Phase 2 (refinement; Eq. (4)). To further probe, we evaluate mechanistic fidelity using the CoarseScore (Phase 1; Eq. 1) and RefineScore (Phase 2; Eq. 3) from Sec. 2, which provide mechanistic views of the above metrics. We also report standard task metrics (e.g., Macro-F1; App. D.2).

RQ1: Do mechanistically distilled students remain more *focused* and less *confused* than ones trained with vanilla CoT distillation? Table 1 compares Focus and Confusion of mechanistically distilled students (LLaMA3-7B, LLaMA3-13B) against CoT distillation baselines on LF-WikiSeeAlso-320K and MIMIC-IV-full, using LLaMA3-70B as the teacher; green rows denote mechanistic distillation, with per-dataset average gains. Baselines achieve partial imitation (LAS), but low Focus and high Confusion show it does not recover the teacher’s coarse-to-fine reasoning. In contrast, mechanistic distillation delivers largest Focus and Confusion gains, showing that transferring Phase 1/2 behaviors via our method brings students closer to the teacher’s reasoning.

RQ2: Do mechanistically distilled students recover the teacher’s phase-specific reasoning mechanisms? Table 1 reports the constituent subscores of CoarseScore (Eq. 1) and RefineScore (Eq. 3), respectively: Phase 1—sharp attention, anchor alignment; Phase 2—QK loop-back, OV helpfulness. Mechanistic distillation recovers both phases: students learn to focus attention on salient tokens (high kurtosis) and write updates that align representations with the semantic anchor, while also re-attending to shortlisted candidates over near-misses and writing updates that increase the target–near-miss margin. In contrast, baselines exhibit diffuse attention, weak anchor alignment, and poor refinement behavior. Gains remain strong but smaller on MIMIC-IV-full than on LF-WikiSeeAlso-320K, likely due to noisier data, longer texts, and the complexity of clinical notes.

RQ3: How do phase-specific losses shape the reasoning dynamics? Figure 1 shows coarse-to-fine reasoning structure in LLaMA3-70B (teacher) and LLaMA3-7B (student) by tracking *cumulative* metrics along the normalized CoT trajectory $t \in [0, 1]$. At each token position $t \leq t^*$, *Reasoning Focus* (left panel; Eq. (2)) measures how strongly the CoT prefix up to t aligns with the dominant semantic anchors $c(x)$, capturing Phase 1 coarse semantic filtering. Conversely, for $t \geq t^*$, *Near-Miss Confusion* (right panel; Eq. (4)) measures how strongly the evolving reasoning prefix—formed by augmenting

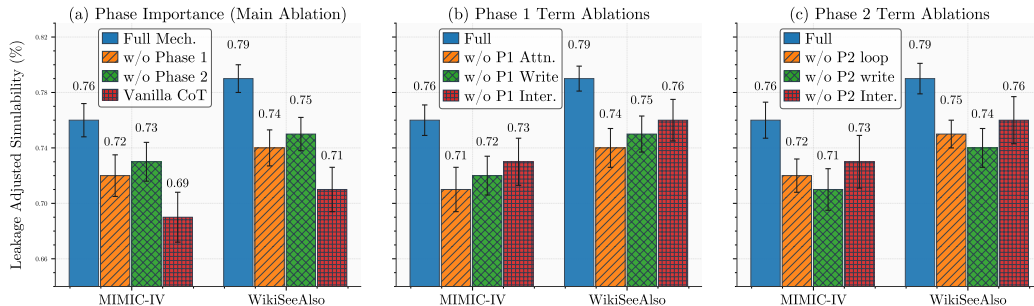


Figure 9: Ablating phases & specific atten./write/interaction losses in Eqs. 5, 6 degrades CoT fidelity.

fixed semantic anchors with progressively generated late CoT tokens—remains aligned with semantically plausible but incorrect alternatives, quantifying Phase 2 contrastive refinement. The teacher exhibits a clear coarse-to-fine structure: rapid focus buildup in early positions followed by progressive reduction in confusion later. Vanilla CoT distillation induces neither phase effectively, producing weak early focus and persistently high late-stage confusion. Phase-specific ablations reveal distinct mechanistic roles—Phase-1-only supervision improves early focus but not late refinement, while Phase-2-only supervision yields limited early focus but some late discrimination. In contrast, full mechanistic distillation (Phase 1&2) closely matches teacher’s trajectory on LF-WikiSeeAlso-320K and MIMIC-IV-full, showing both objectives are complementary & necessary.

Ablation Analysis To better understand the contribution of our mechanistic distillation framework, we conduct an ablation study on the *LAS* metric [Wang et al., 2023], which measures how faithfully the student’s generated rationale recovers the teacher’s gold answer. Figure 9 presents the results across MIMIC-IV-full and LF-WikiSeeAlso-320K datasets. Panel (a) ablates entire phases, showing that removing either Phase 1 (coarse filtering) or Phase 2 (iterative refinement) substantially degrades CoT fidelity. Panels (b) and (c) further break down the three-term decomposition of each phase’s loss (attention/QK, write/OV, and their multiplicative interaction in Eqs. 5, 6). These results demonstrate that all components are important, with the interaction terms consistently contributing strong complementary gains. Overall, the full mechanistic distillation objective yields the highest teacher faithfulness, validating our phase-specific pooled-head distillation design.

5 Related Work

Recent CoT distillation improve smaller reasoning models by transferring teacher-generated rationales, often through better rationale selection, structural supervision, or more efficient reasoning representations. For example, Zhuang et al. [2025] distills structured reasoning trajectories beyond linear CoT, Yan et al. [2025] improves data efficiency through rationale selection, He et al. [2026] replaces explicit reasoning traces with semantically aligned implicit tokens, while Xu et al. [2025b] performs reasoning in a continuous latent space using soft thought tokens, and Chen et al. [2025c] compresses reasoning by distilling chunk-wise CoT execution. Related work studies efficient reasoning supervision through rationale pruning, implicit reasoning tokens, and compressed CoT representations [Deng et al., 2023, Cheng and Van Durme, 2024, Feng et al., 2024, Wei et al., 2025, Fan et al., 2025, Shen et al., 2025, Kang et al., 2025b]. However, they do not explore large space reasoning and treat reasoning traces as supervision target, focusing on *what* reasoning text to transfer. In contrast, we study *how* reasoning is internally implemented and distill the underlying mechanisms.

Our work is also related to mechanistic interpretability and representation-level distillation. Prior studies use attention decomposition to identify functional transformer components and analyze reasoning behavior [Dutta et al., 2024, Cabannes et al., 2024, Chen et al., 2025b]. Recent work further reveals specialized attention heads, including retrieval heads that enable long-context factuality and information copying [Wu et al., 2024], heterogeneous attention spans across heads for efficient inference [Fu et al., 2025], and retrieval heads that enable aggressive KV cache compression while preserving performance [Tang et al., 2024]. A comprehensive survey of attention head functions in LLMs [Zheng et al., 2024] further categorizes their roles in knowledge recalling, in-context identification, latent reasoning, and expression preparation. We connect these directions by first characterizing reasoning in large label spaces as a two-phase process and then distilling these phases through mechanism-specific objectives over attention patterns and residual updates.

References

- Samyadeep Basu, Vlad I. Morariu, Ryan A. Rossi, Nanxuan Zhao, Zichao Wang, Soheil Feizi, and Varun Manjunatha. On Mechanistic Circuits for Extractive Question-Answering. August 2025. URL <https://openreview.net/forum?id=VvSWiNuPL#discussion>.
- Leonard Bereska and Efstratios Gavves. Mechanistic Interpretability for AI Safety – A Review, August 2024. URL <http://arxiv.org/abs/2404.14082>. arXiv:2404.14082 [cs].
- Maciej Besta, Julia Barth, Eric Schreiber, Ales Kubicek, Afonso Catarino, Robert Gerstenberger, Piotr Nyczyk, Patrick Iff, Yueling Li, Sam Houliston, Tomasz Sternal, Marcin Copik, Grzegorz Kwaśniewski, Jürgen Müller, Łukasz Flis, Hannes Eberhard, Zixuan Chen, Hubert Niewiadomski, and Torsten Hoefler. Reasoning Language Models: A Blueprint, June 2025. URL <http://arxiv.org/abs/2501.11223>. arXiv:2501.11223 [cs].
- Vivien Cabannes, Charles Arnal, Wassim Bouaziz, Alice Yang, Francois Charton, and Julia Kempe. Iteration head: A mechanistic study of chain-of-thought. *Advances in Neural Information Processing Systems*, 37:109101–109122, 2024.
- Qiguang Chen, Libo Qin, Jinhao Liu, Dengyun Peng, Jiannan Guan, Peng Wang, Mengkang Hu, Yuhang Zhou, Te Gao, and Wanxiang Che. Towards Reasoning Era: A Survey of Long Chain-of-Thought for Reasoning Large Language Models, July 2025a. URL <http://arxiv.org/abs/2503.09567>. arXiv:2503.09567 [cs].
- Qiguang Chen, Yantao Du, Ziniu Li, Jinhao Liu, Songyao Duan, Jiarui Guo, Minghao Liu, Jiaheng Liu, Tong Yang, Ge Zhang, Libo Qin, Wanxiang Che, and Wenhao Huang. The Molecular Structure of Thought: Mapping the Topology of Long Chain-of-Thought Reasoning, January 2026. URL <http://arxiv.org/abs/2601.06002>. arXiv:2601.06002 [cs].
- Xi Chen, Aske Plaat, and Niki van Stein. How does Chain of Thought Think? Mechanistic Interpretability of Chain-of-Thought Reasoning with Sparse Autoencoding, July 2025b. URL <http://arxiv.org/abs/2507.22928>. arXiv:2507.22928 [cs].
- Xiaoshu Chen, Sihang Zhou, Ke Liang, Xiaoyu Sun, and Xinwang Liu. Skip-Thinking: Chunk-wise Chain-of-Thought Distillation Enable Smaller Language Models to Reason Better and Faster. In Christos Christodoulopoulos, Tanmoy Chakraborty, Carolyn Rose, and Violet Peng, editors, *Proceedings of the 2025 Conference on Empirical Methods in Natural Language Processing*, pages 12142–12157, Suzhou, China, November 2025c. Association for Computational Linguistics. ISBN 979-8-89176-332-6. doi: 10.18653/v1/2025.emnlp-main.610. URL <https://aclanthology.org/2025.emnlp-main.610/>.
- Xinghao Chen, Zhijing Sun, Wenjin Guo, Miaoran Zhang, Yanjun Chen, Yirong Sun, Hui Su, Yijie Pan, Dietrich Klakow, Wenjie Li, and Xiaoyu Shen. Unveiling the Key Factors for Distilling Chain-of-Thought Reasoning, May 2025d. URL <http://arxiv.org/abs/2502.18001>. arXiv:2502.18001 [cs].
- Jeffrey Cheng and Benjamin Van Durme. Compressed chain of thought: Efficient reasoning through dense representations. *arXiv preprint arXiv:2412.13171*, 2024.
- Yu-Neng Chuang, Guanchu Wang, Chia-Yuan Chang, Ruixiang Tang, Shaochen Zhong, Fan Yang, Mengnan Du, Xuanning Cai, Vladimir Braverman, and Xia Hu. FaithLM: Towards Faithful Explanations for Large Language Models, October 2025. URL <http://arxiv.org/abs/2402.04678>. arXiv:2402.04678 [cs].
- Kunal Dahiya, Diego Ortego, and David Jimenez-Cabello. Prototypical Extreme Multi-label Classification with a Dynamic Margin Loss. In Luis Chiruzzo, Alan Ritter, and Lu Wang, editors, *Proceedings of the 2025 Conference of the Nations of the Americas Chapter of the Association for Computational Linguistics: Human Language Technologies (Volume 1: Long Papers)*, pages 10709–10727, Albuquerque, New Mexico, April 2025. Association for Computational Linguistics. ISBN 979-8-89176-189-6. doi: 10.18653/v1/2025.naacl-long.537. URL <https://aclanthology.org/2025.naacl-long.537/>.

- Chengwei Dai, Kun Li, Wei Zhou, and Songlin Hu. Beyond Imitation: Learning Key Reasoning Steps from Dual Chain-of-Thoughts in Reasoning Distillation, May 2024. URL <http://arxiv.org/abs/2405.19737>. arXiv:2405.19737 [cs].
- Janez Demšar. Statistical comparisons of classifiers over multiple data sets. *Journal of Machine Learning Research*, 7(Jan):1–30, 2006.
- Yuntian Deng, Kiran Prasad, Roland Fernandez, Paul Smolensky, Vishrav Chaudhary, and Stuart Shieber. Implicit chain of thought reasoning via knowledge distillation. *arXiv preprint arXiv:2311.01460*, 2023.
- Hongzhe Du, Weikai Li, Min Cai, Karim Saraipour, Zimin Zhang, Himabindu Lakkaraju, Yizhou Sun, and Shichang Zhang. How Post-Training Reshapes LLMs: A Mechanistic View on Knowledge, Truthfulness, Refusal, and Confidence, November 2025. URL <http://arxiv.org/abs/2504.02904>. arXiv:2504.02904 [cs].
- Subhabrata Dutta, Joykirat Singh, Soumen Chakrabarti, and Tanmoy Chakraborty. How to think step-by-step: A mechanistic understanding of chain-of-thought reasoning, May 2024. URL <http://arxiv.org/abs/2402.18312>. arXiv:2402.18312 [cs].
- Siqi Fan, Peng Han, Shuo Shang, Yequan Wang, and Aixin Sun. Cothink: Token-efficient reasoning via instruct models guiding reasoning models. *arXiv e-prints*, pages arXiv–2505, 2025.
- Luyang Fang, Xiaowei Yu, Jiazhang Cai, Yongkai Chen, Shushan Wu, Zhengliang Liu, Zhenyuan Yang, Haoran Lu, Xilin Gong, Yufang Liu, Terry Ma, Wei Ruan, Ali Abbasi, Jing Zhang, Tao Wang, Ehsan Latif, Weihang You, Hanqi Jiang, Wei Liu, Wei Zhang, Soheil Kolouri, Xiaoming Zhai, Dajiang Zhu, Wenxuan Zhong, Tianming Liu, and Ping Ma. Knowledge Distillation and Dataset Distillation of Large Language Models: Emerging Trends, Challenges, and Future Directions, January 2026. URL <http://arxiv.org/abs/2504.14772>. arXiv:2504.14772 [cs].
- Kaituo Feng, Changsheng Li, Xiaolu Zhang, Jun Zhou, Ye Yuan, and Guoren Wang. Keypoint-based Progressive Chain-of-Thought Distillation for LLMs, May 2024. URL <http://arxiv.org/abs/2405.16064>. arXiv:2405.16064 [cs].
- Tianyu Fu, Haofeng Huang, Xuefei Ning, Genghan Zhang, Boju Chen, Tianqi Wu, Hongyi Wang, Zixiao Huang, Shiyao Li, Shengen Yan, Guohao Dai, Huazhong Yang, and Yu Wang. Mixture of Attention Spans: Optimizing LLM Inference Efficiency with Heterogeneous Sliding-Window Lengths, November 2025. URL <http://arxiv.org/abs/2406.14909>. arXiv:2406.14909 [cs].
- Atticus Geiger, Duligur Ibeling, Amir Zur, Maheep Chaudhary, Sonakshi Chauhan, Jing Huang, Aryaman Arora, Zhengxuan Wu, Noah Goodman, Christopher Potts, and Thomas Icard. Causal Abstraction: A Theoretical Foundation for Mechanistic Interpretability, May 2025. URL <http://arxiv.org/abs/2301.04709>. arXiv:2301.04709 [cs].
- Melody Y. Guan, Manas Joglekar, Eric Wallace, Saachi Jain, Boaz Barak, Alec Helyar, Rachel Dias, Andrea Vallone, Hongyu Ren, Jason Wei, Hyung Won Chung, Sam Toyer, Johannes Heidecke, Alex Beutel, and Amelia Glaese. Deliberative Alignment: Reasoning Enables Safer Language Models, January 2025. URL <http://arxiv.org/abs/2412.16339>. arXiv:2412.16339 [cs].
- Daya Guo, Dejian Yang, Haowei Zhang, Junxiao Song, Ruoyu Zhang, Runxin Xu, Qihao Zhu, Shirong Ma, Peiyi Wang, Xiao Bi, et al. Deepseek-r1: Incentivizing reasoning capability in llms via reinforcement learning. *arXiv preprint arXiv:2501.12948*, 2025. URL <https://arxiv.org/abs/2501.12948>.
- Nilesh Gupta, Devvrit Khatri, Ankit S. Rawat, Srinadh Bhojanapalli, Prateek Jain, and Inderjit Dhillon. Dual-Encoders for Extreme Multi-Label Classification, March 2024. URL <http://arxiv.org/abs/2310.10636>. arXiv:2310.10636 [cs] version: 2.
- Michael Hanna, Sandro Pezzelle, and Yonatan Belinkov. Have Faith in Faithfulness: Going Beyond Circuit Overlap When Finding Model Mechanisms, July 2024. URL <http://arxiv.org/abs/2403.17806>. arXiv:2403.17806 [cs].

- Yinhan He, Wendy Zheng, Yaochen Zhu, Zaiyi Zheng, Lin Su, Sriram Vasudevan, Qi Guo, Liangjie Hong, and Jundong Li. SemCoT: Accelerating Chain-of-Thought Reasoning through Semantically-Aligned Implicit Tokens, 2025. URL <https://arxiv.org/abs/2510.24940>. Version Number: 3.
- Yinhan He, Wendy Zheng, Yaochen Zhu, Zaiyi Zheng, Lin Su, Sriram Vasudevan, Qi Guo, Liangjie Hong, and Jundong Li. SemCoT: Accelerating Chain-of-Thought Reasoning through Semantically-Aligned Implicit Tokens, January 2026. URL <http://arxiv.org/abs/2510.24940>. arXiv:2510.24940 [cs].
- Stefan Heimersheim and Neel Nanda. How to use and interpret activation patching, April 2024. URL <http://arxiv.org/abs/2404.15255>. arXiv:2404.15255 [cs].
- Cheng-Ping Hsieh, Simeng Sun, Samuel Kriman, Shantanu Acharya, Dima Rekesh, Fei Jia, Yang Zhang, and Boris Ginsburg. RULER: What’s the Real Context Size of Your Long-Context Language Models?, August 2024. URL <http://arxiv.org/abs/2404.06654>. arXiv:2404.06654 [cs].
- Yueqing Hu, Xinyang Peng, Shuting Peng, Hanqi Wang, and Tianhong Wang. Hán Dān Xué Bù (Mimicry) or Qīng Chū Yú Lán (Mastery)? A Cognitive Perspective on Reasoning Distillation in Large Language Models, January 2026. URL <http://arxiv.org/abs/2601.05019>. arXiv:2601.05019 [cs].
- Yixin Ji, Juntao Li, Hai Ye, Kaixin Wu, Jia Xu, Linjian Mo, and Min Zhang. Test-time computing: from system-1 thinking to system-2 thinking. *arXiv e-prints*, pages arXiv–2501, 2025. URL <https://arxiv.org/pdf/2501.02497v1>.
- Alistair EW Johnson, Lucas Bulgarelli, Lu Shen, Alvin Gayles, Ayad Shammout, Steven Horng, Tom J Pollard, Sicheng Hao, Benjamin Moody, Brian Gow, et al. Mimic-iv, a freely accessible electronic health record dataset. *Scientific data*, 10(1):1, 2023.
- Greg Kamradt. Needle in a haystack – pressure testing llms. https://github.com/gkamradt/LLMTest_NeedleInAHaystack, 2023. GitHub repository.
- Minki Kang, Jongwon Jeong, Seanie Lee, Jaewoong Cho, and Sung Ju Hwang. Distilling LLM Agent into Small Models with Retrieval and Code Tools, November 2025a. URL <http://arxiv.org/abs/2505.17612>. arXiv:2505.17612 [cs].
- Yu Kang, Xianghui Sun, Liangyu Chen, and Wei Zou. C3ot: Generating shorter chain-of-thought without compromising effectiveness. In *Proceedings of the AAAI Conference on Artificial Intelligence*, volume 39, pages 24312–24320, 2025b.
- Yuri Kuratov, Aydar Bulatov, Petr Anokhin, Ivan Rodkin, Dmitry Sorokin, Artyom Sorokin, and Mikhail Burtsev. BABILong: Testing the Limits of LLMs with Long Context Reasoning-in-a-Haystack, November 2024. URL <http://arxiv.org/abs/2406.10149>. arXiv:2406.10149 [cs].
- Dacheng Li, Shiyi Cao, Tyler Griggs, Shu Liu, Xiangxi Mo, Eric Tang, Sumanth Hegde, Kourosh Hakhmaneshi, Shishir G. Patil, Matei Zaharia, Joseph E. Gonzalez, and Ion Stoica. LLMs Can Easily Learn to Reason from Demonstrations Structure, not content, is what matters!, February 2025a. URL <http://arxiv.org/abs/2502.07374>. arXiv:2502.07374 [cs].
- Zhong-Zhi Li, Duzhen Zhang, Ming-Liang Zhang, Jiaxin Zhang, Zengyan Liu, Yuxuan Yao, Haotian Xu, Junhao Zheng, Pei-Jie Wang, Xiuyi Chen, Yingying Zhang, Fei Yin, Jiahua Dong, Zhiwei Li, Bao-Long Bi, Ling-Rui Mei, Junfeng Fang, Xiao Liang, Zhijiang Guo, Le Song, and Cheng-Lin Liu. From System 1 to System 2: A Survey of Reasoning Large Language Models, June 2025b. URL <http://arxiv.org/abs/2502.17419>. arXiv:2502.17419 [cs].
- Nelson F. Liu, Kevin Lin, John Hewitt, Ashwin Paranjape, Michele Bevilacqua, Fabio Petroni, and Percy Liang. Lost in the Middle: How Language Models Use Long Contexts, November 2023. URL <http://arxiv.org/abs/2307.03172>. arXiv:2307.03172 [cs].

- Sara Vera Marjanović, Arkil Patel, Vaibhav Adlakha, Milad Aghajohari, Parishad BehnamGhader, Mehar Bhatia, Aditi Khandelwal, Austin Kraft, Benno Krojer, Xing Han Lù, Nicholas Meade, Dongchan Shin, Amirhossein Kazemnejad, Gaurav Kamath, Marius Mosbach, Karolina Stańczak, and Siva Reddy. DeepSeek-R1 Thoughtology: Let’s think about LLM Reasoning, January 2026. URL <http://arxiv.org/abs/2504.07128>. arXiv:2504.07128 [cs].
- Eric J. Michaud, Isaac Liao, Vedang Lad, Ziming Liu, Anish Mudide, Chloe Loughridge, Zifan Carl Guo, Tara Rezaei Kheirkhah, Mateja Vukelić, and Max Tegmark. Opening the AI black box: program synthesis via mechanistic interpretability, February 2024. URL <http://arxiv.org/abs/2402.05110>. arXiv:2402.05110 [cs].
- Ali Modarressi, Hanieh Deilamsalehy, Franck Deroncourt, Trung Bui, Ryan A. Rossi, Seunghyun Yoon, and Hinrich Schütze. NoLiMa: Long-Context Evaluation Beyond Literal Matching, July 2025. URL <http://arxiv.org/abs/2502.05167>. arXiv:2502.05167 [cs].
- Neel Nanda, Lawrence Chan, Tom Lieberum, Jess Smith, and Jacob Steinhardt. Progress measures for grokking via mechanistic interpretability, October 2023. URL <http://arxiv.org/abs/2301.05217>. arXiv:2301.05217 [cs].
- OpenAI. Introducing openai o3 and o4-mini, April 2025a. URL <https://openai.com/index/introducing-o3-and-o4-mini/>. Announcement date: April 16, 2025.
- OpenAI. Introducing gpt-5.2, December 2025b. URL <https://openai.com/index/introducing-gpt-5-2/>. Announcement date: December 11, 2025.
- Diego Ortego, Marlon Rodríguez, Mario Almagro, Kunal Dahiya, David Jiménez, and Juan C. SanMiguel. Large Language Models Meet Extreme Multi-label Classification: Scaling and Multi-modal Framework, November 2025. URL <http://arxiv.org/abs/2511.13189>. arXiv:2511.13189 [cs].
- Suhas Kamasetty Ramesh, Ayan Sengupta, and Tanmoy Chakraborty. On the Generalization vs Fidelity Paradox in Knowledge Distillation, August 2025. URL <http://arxiv.org/abs/2505.15442>. arXiv:2505.15442 [cs].
- Zhenyi Shen, Hanqi Yan, Linhai Zhang, Zhanghao Hu, Yali Du, and Yulan He. Codi: Compressing chain-of-thought into continuous space via self-distillation. In *Proceedings of the 2025 Conference on Empirical Methods in Natural Language Processing*, pages 677–693, 2025.
- Alessandro Stolfo, Yonatan Belinkov, and Mrinmaya Sachan. A Mechanistic Interpretation of Arithmetic Reasoning in Language Models using Causal Mediation Analysis, October 2023. URL <http://arxiv.org/abs/2305.15054>. arXiv:2305.15054 [cs].
- Seyed Amin Tabatabaei, Sarah Fancher, Michael Parsons, and Arian Askari. Can Large Language Models Serve as Effective Classifiers for Hierarchical Multi-Label Classification of Scientific Documents at Industrial Scale? In Owen Rambow, Leo Wanner, Marianna Apidianaki, Hend Al-Khalifa, Barbara Di Eugenio, Steven Schockaert, Kareem Darwish, and Apoorv Agarwal, editors, *Proceedings of the 31st International Conference on Computational Linguistics: Industry Track*, pages 163–174, Abu Dhabi, UAE, January 2025. Association for Computational Linguistics. URL <https://aclanthology.org/2025.coling-industry.14/>.
- Zhen Tan, Chengshuai Zhao, Song Wang, Jundong Li, Tianlong Chen, and Huan Liu. Probing to Refine: Reinforcement Distillation of LLMs via Explanatory Inversion, February 2026. URL <https://arxiv.org/abs/2603.19266v1>.
- Hanlin Tang, Yang Lin, Jing Lin, Qingsen Han, Shikuan Hong, Yiwu Yao, and Gongyi Wang. RazorAttention: Efficient KV Cache Compression Through Retrieval Heads, July 2024. URL <http://arxiv.org/abs/2407.15891>. arXiv:2407.15891 [cs].
- Somin Wadhwa, Silvio Amir, and Byron C Wallace. Investigating mysteries of CoT-augmented distillation. In Yaser Al-Onaizan, Mohit Bansal, and Yun-Nung Chen, editors, *Proceedings of the 2024 Conference on Empirical Methods in Natural Language Processing*, pages 6071–6086, Miami, Florida, USA, November 2024. Association for Computational Linguistics. doi: 10.18653/v1/2024.emnlp-main.349. URL <https://aclanthology.org/2024.emnlp-main.349/>.

- Peifeng Wang, Zhengyang Wang, Zheng Li, Yifan Gao, Bing Yin, and Xiang Ren. SCOTT: Self-Consistent Chain-of-Thought Distillation, August 2023. URL <http://arxiv.org/abs/2305.01879>. arXiv:2305.01879 [cs].
- Yidong Wang. Reasoning on Multiple Needles In A Haystack, April 2025. URL <http://arxiv.org/abs/2504.04150>. arXiv:2504.04150 [cs].
- Xilin Wei, Xiaoran Liu, Yuhang Zang, Xiaoyi Dong, Yuhang Cao, Jiaqi Wang, Xipeng Qiu, and Dahua Lin. Sim-cot: Supervised implicit chain-of-thought. *arXiv preprint arXiv:2509.20317*, 2025.
- Peter H Westfall. Kurtosis as peakedness, 1905–2014. rip. *The American Statistician*, 68(3):191–195, 2014.
- WHO. *International Statistical Classification of Diseases and Related Health Problems*. 11th edition, 2025. URL <https://www.who.int/standards/classifications/classification-of-diseases>.
- Wenhao Wu, Yizhong Wang, Guangxuan Xiao, Hao Peng, and Yao Fu. Retrieval Head Mechanistically Explains Long-Context Factuality, April 2024. URL <http://arxiv.org/abs/2404.15574>. arXiv:2404.15574 [cs].
- Fengli Xu, Qian Yue Hao, Zefang Zong, Jingwei Wang, Yunke Zhang, Jingyi Wang, Xiaochong Lan, Jiahui Gong, Tianjian Ouyang, Fanjin Meng, Chenyang Shao, Yuwei Yan, Qinglong Yang, Yiwen Song, Sijian Ren, Xinyuan Hu, Yu Li, Jie Feng, Chen Gao, and Yong Li. Towards Large Reasoning Models: A Survey of Reinforced Reasoning with Large Language Models, January 2025a. URL <http://arxiv.org/abs/2501.09686>. arXiv:2501.09686 [cs].
- Yige Xu, Xu Guo, Zhiwei Zeng, and Chunyan Miao. Softcot: Soft chain-of-thought for efficient reasoning with llms. In *Proceedings of the 63rd Annual Meeting of the Association for Computational Linguistics (Volume 1: Long Papers)*, pages 23336–23351, 2025b.
- JianZhi Yan, Le Liu, Youcheng Pan, Shiwei Chen, Yang Xiang, and Buzhou Tang. Towards Efficient CoT Distillation: Self-Guided Rationale Selector for Better Performance with Fewer Rationales. In Christos Christodoulopoulos, Tanmoy Chakraborty, Carolyn Rose, and Violet Peng, editors, *Findings of the Association for Computational Linguistics: EMNLP 2025*, pages 7818–7835, Suzhou, China, November 2025. Association for Computational Linguistics. ISBN 979-8-89176-335-7. doi: 10.18653/v1/2025.findings-emnlp.413. URL <https://aclanthology.org/2025.findings-emnlp.413/>.
- Shunyu Yao, Dian Yu, Jeffrey Zhao, Izhak Shafran, Thomas L. Griffiths, Yuan Cao, and Karthik Narasimhan. Tree of Thoughts: Deliberate Problem Solving with Large Language Models, December 2023. URL <http://arxiv.org/abs/2305.10601>. arXiv:2305.10601 [cs].
- Edward Yeo, Yuxuan Tong, Morry Niu, Graham Neubig, and Xiang Yue. Demystifying Long Chain-of-Thought Reasoning in LLMs, February 2025. URL <http://arxiv.org/abs/2502.03373>. arXiv:2502.03373 [cs].
- Jinbin Zhang, Nasib Ullah, Erik Schultheis, and Rohit Babbar. ELMO: Efficiency via Low-precision and Peak Memory Optimization in Large Output Spaces, October 2025. URL <http://arxiv.org/abs/2510.11168>. arXiv:2510.11168 [cs].
- Yadong Zhang, Shaoguang Mao, Tao Ge, Xun Wang, Adrian de Wynter, Yan Xia, Wenshan Wu, Ting Song, Man Lan, and Furu Wei. LLM as a Mastermind: A Survey of Strategic Reasoning with Large Language Models, April 2024. URL <http://arxiv.org/abs/2404.01230>. arXiv:2404.01230 [cs].
- Zifan Zheng, Yezhaohui Wang, Yuxin Huang, Shichao Song, Mingchuan Yang, Bo Tang, Feiyu Xiong, and Zhiyu Li. Attention Heads of Large Language Models: A Survey, December 2024. URL <http://arxiv.org/abs/2409.03752>. arXiv:2409.03752 [cs].

Chuang Zhou, Junnan Dong, Xiao Huang, Zirui Liu, Kaixiong Zhou, and Zhaozhuo Xu. QUEST: Efficient Extreme Multi-Label Text Classification with Large Language Models on Commodity Hardware. In Yaser Al-Onaizan, Mohit Bansal, and Yun-Nung Chen, editors, *Findings of the Association for Computational Linguistics: EMNLP 2024*, pages 3929–3940, Miami, Florida, USA, November 2024. Association for Computational Linguistics. doi: 10.18653/v1/2024.findings-emnlp.226. URL <https://aclanthology.org/2024.findings-emnlp.226/>.

Xianwei Zhuang, Zhihong Zhu, Zhichang Wang, Xuxin Cheng, and Yuexian Zou. UNICOTT: A UNIFIED FRAMEWORK FOR STRUCTURAL CHAIN-OF-THOUGHT DISTILLATION. 2025.

A Training Details

Models. We use publicly available open-weight large language models as both teachers and students. Our primary teacher model is LLaMA3-70B, while student models include smaller open-weight architectures such as LLaMA3-7B. Additional model variants used in ablations and scaling experiments are described in Sec. 4.

Datasets. Experiments are conducted on publicly available large-scale multi-label datasets spanning clinical coding and extreme multi-label retrieval settings. These include MIMIC-IV-full, MIMIC-III-full, and LF-WikiSeeAlso-320K. We use the standard train/dev/test splits provided by prior work for all datasets.

Training setup. All experiments are conducted on 8xA100-80GB GPUs using DeepSpeed ZeRO-3 offloading for memory efficiency and distributed training. Models are trained using mixed-precision FP16 training with gradient accumulation.

For mechanistic distillation, both teacher and student are run under teacher forcing on the same reasoning trajectories to enable aligned phase-wise supervision. Training combines the standard chain-of-thought distillation objective with our proposed mechanistic losses: (i) Phase 1 coarse semantic focusing supervision and (ii) Phase 2 contrastive refinement supervision.

Optimization. We optimize all models using AdamW with cosine learning-rate scheduling and linear warmup. Hyperparameters are selected based on validation performance on the development split. Gradient clipping is applied for training stability.

Mechanistic supervision. Phase 1 supervision operates over early reasoning positions identified using the temporal reasoning trajectory described in Sec. 2. Heads are ranked using CoarseScore and pooled to form phase-level supervision targets.

Phase 2 supervision operates over mid-to-late reasoning positions corresponding to refinement behavior. Heads are ranked using RefineScore and used to supervise shortlist retrieval and margin-widening refinement behavior.

Activation patching. For mechanistic validation, we perform both denoising and noising activation patching over attention heads ranked by the proposed phase-specific metrics. Patching experiments are conducted independently from training and are used solely for causal analysis.

Evaluation metrics. We report standard extreme multi-label classification metrics including macro-F1, Precision@ k , and propensity-scored metrics where applicable. For mechanistic evaluation, we additionally report trajectory-based reasoning metrics including *Focus* and *Near-Miss Confusion*.

Statistical significance. Following prior work, we evaluate statistical significance using paired Wilcoxon signed-rank testing. Additional details are provided in App. E.

Reproducibility. We release anonymized code and training scripts at submission time: <https://github.com/research-anon-487/xcube/tree/reasoning>. The repository contains preprocessing scripts, training pipelines, mechanistic analysis utilities, and evaluation commands required to reproduce the primary experiments. Trained checkpoints will be released upon acceptance.

B Mathematical Details

Reasoning Focus

To quantify the progressive alignment of early reasoning with the core clinical signals, we define the reasoning focus metric. For each input x , we first precompute a compact broad-category representation $c(x)$ that captures the dominant high-level semantic signals (e.g., systolic heart failure, volume overload, cardiorenal syndrome). This is obtained in one of two ways:

When ground-truth labels $L(x)$ are available, $c(x)$ is the centroid of the embeddings of the true labels (or their ontological ancestors):

$$c(x) = \frac{1}{|L(x)|} \sum_{\ell \in L(x)} e(\ell).$$

When ground-truth labels are unavailable, $c(x) = e(\text{LLM}_{\text{summary}}(x))$, where a frozen auxiliary LLM extracts a short list of key clinical concepts from x .

Let r_1, r_2, \dots, r_K denote the tokens of the early CoT segment. We then define the focus after the first k tokens as the average cosine similarity with the broad-category vector:

$$\text{Focus}(k) = \frac{1}{k} \sum_{q=1}^k \cos(e(r_q), c(x)).$$

Intuition: This construction captures progressive semantic alignment: early CoT tokens are initially diffuse and may reflect surface-level cues or partial hypotheses, yielding weaker alignment with the dominant signal $c(x)$. As reasoning unfolds, tokens increasingly consolidate around the core clinical concepts, causing the cumulative average to rise. Strong models therefore exhibit a clear increasing trajectory in $\text{Focus}(k)$ as k grows, reflecting rapid convergence toward the correct semantic anchors, while weaker or distilled models show slower growth or lower saturation, indicating less coherent early-stage reasoning.

Near-Miss Confusion

To quantify how effectively late-stage contrastive reasoning suppresses near-miss alternatives, we define the near-miss confusion metric. For each input x , we first extract a fixed set of broad semantic anchors $\mathcal{A}(x)$ (e.g., “systolic heart failure”, “volume overload”, “cardiorenal syndrome”, “EF 35%”, etc.). We then create a short fixed anchor text $a(x)$ that explicitly lists or summarizes these anchors (this is the same textual representation used for the Focus metric in early reasoning).

Then, let $n(x)$ be the centroid of the near-miss categories $\mathcal{N}(x)$ (e.g., HFpEF, pneumonia, primary renal failure, isolated AKI, etc.):

$$n(x) = \frac{1}{|\mathcal{N}(x)|} \sum_{m \in \mathcal{N}(x)} e(m).$$

Let r_1, \dots, r_K be the tokens of the late (contrastive/refinement) CoT segment. For each $k = 1, \dots, K$, we form the cumulative prefix

$$s_k = a(x) \parallel [r_1 \dots r_k],$$

i.e., we append the progressive late CoT tokens to the fixed anchor text. The near-miss confusion after k late tokens is

$$\text{Confusion}(k) = \frac{1}{k} \sum_{q=1}^k \cos(e(s_q), n(x)).$$

Intuition: This cumulative construction is intentional: the anchor text $a(x)$ alone captures only broad categories and therefore still has non-negligible similarity to many near-misses. Only when the late contrastive tokens (explicitly ruling out competitors) are appended does the full prefix s_k pull away from $n(x)$. Strong models therefore show a clear decreasing trajectory in $\text{Confusion}(k)$ versus k , while distilled models exhibit flatter or slower decay.

Computing $\text{avg_logit}_{\text{target}}(q)$

At a refinement token position q , we compute the average target logit as follows.

First, run the model’s forward pass up to position q and obtain the final residual stream representation $h_{\text{final}}(q)$. The vocabulary logits at this position are computed by applying the model’s unembedding matrix:

$$\text{logits}(q) = W_{\text{unembed}} h_{\text{final}}(q) + b,$$

where $\text{logits}(q) \in \mathbb{R}^{|\mathcal{V}|}$ contains scores for all vocabulary tokens.

Next, identify the target labels in the shortlist. These correspond to the ground-truth positive labels (or the correct shortlist subcategories identified by the model), such as “acute pancreatitis” or “NBA playoff overtime rules”. Suppose there are k such targets with token IDs

$$\text{label_ids}_{\text{target}} = [id_1, id_2, \dots, id_k].$$

The average target logit at position q is then computed as

$$\text{avg_logit}_{\text{target}}(q) = \frac{1}{k} \sum_{i=1}^k \text{logits}(q)[\text{label_ids}_{\text{target}}[i]].$$

This quantity represents the mean logit value among the correct labels at position q .

We compute an analogous quantity for the near-miss labels (e.g., “chronic pancreatitis”, “regular season tiebreaker”). If their token IDs are

$$\text{label_ids}_{\text{near_miss}} = [id_1, id_2, \dots, id_m],$$

then

$$\text{avg_logit}_{\text{near_miss}}(q) = \frac{1}{m} \sum_{j=1}^m \text{logits}(q)[\text{label_ids}_{\text{near_miss}}[j]].$$

Finally, we define the margin at position q as the scalar difference

$$\text{margin}(q) = \text{avg_logit}_{\text{target}}(q) - \text{avg_logit}_{\text{near_miss}}(q). \quad (7)$$

This quantity measures how strongly the model favors the correct shortlist labels over the competing near-miss labels at that refinement step. Lower/negative margin means the model still finds near-misses plausible; higher/positive margin means refinement has widened the gap in favor of the target.

Stable Computation of Pooled Kurtosis.

The Phase 1 **interaction term** (cf. Eq. 5) uses the excess kurtosis of the pooled attention distribution (Eq. 1). To ensure numerical stability, we compute kurtosis on the normalized pooled attention vector $\bar{\alpha}_{q,\cdot}$, which is already a probability distribution produced by the softmax attention mechanism. Let $\bar{\alpha}_{q,\cdot} = (\alpha_1, \dots, \alpha_n)$ denote the pooled attention over all key positions for a query q . We compute excess kurtosis using the standard moment-based estimator

$$\kappa(\bar{\alpha}_{q,\cdot}) = \frac{\frac{1}{n} \sum_{i=1}^n (\alpha_i - \mu)^4}{\left(\frac{1}{n} \sum_{i=1}^n (\alpha_i - \mu)^2 + \epsilon\right)^2} - 3, \quad \mu = \frac{1}{n} \sum_{i=1}^n \alpha_i,$$

where ϵ is a small constant (10^{-6} in our implementation) added for numerical stability.

This computation is well behaved in practice for two reasons. First, attention vectors are normalized and bounded in $[0, 1]$, preventing large moment magnitudes. Second, the stabilization constant in the denominator avoids division by very small variances when the distribution approaches uniformity. As the kurtosis term appears only in the interaction objective and the primary routing supervision is provided by the pooled-attention KL loss (Eq. 5), this statistic acts as a stable auxiliary signal preserving the coarse-filtering structure identified in our mechanistic analysis. Our implementation follows the standard moment-based definition of excess kurtosis used in statistical analysis [Westfall, 2014].

Phase 2 Mechanistic Distillation

Phase 2 heads refine decisions by repeatedly re-attending to previously mentioned shortlist representations while suppressing near-miss alternatives (cf. Eq. 3). To distill this loop-back behavior, we pool query–key similarity scores using the head sets and weights defined above. For $M \in \{T, S\}$ we define $R^M(q) = \sum_h w_h^M \left(\mathbb{E}_{p \in \mathcal{S}(x)} \cos(\mathbf{q}_q^{M,h}, \mathbf{k}_p^{M,h}) - \mathbb{E}_{p \in \mathcal{N}(x)} \cos(\mathbf{q}_q^{M,h}, \mathbf{k}_p^{M,h}) \right)$, $h \in \mathcal{H}_{p_2}^M$, which measures how strongly pooled Phase 2 heads re-attend to shortlist representations while avoiding near-miss ones. Phase 2 heads also write residual updates that widen the margin between target and near-miss labels via the OV circuit (cf. Eq. 3). To distill this behavior, we pool write vectors using the Phase 2 head sets and weights defined above: $\bar{\Delta}^M(q) = \sum_h w_h^M \Delta^{M,h}(q)$, $h \in \mathcal{H}_{p_2}^M$, $M \in \{T, S\}$. We then compute the pooled OV-helpfulness score $H^M(q) = \left\langle \bar{\Delta}^M(q), \nabla_{\mathbf{h}_{\text{final}}(q)} \text{margin}(q) \right\rangle$, which measures how strongly pooled write updates increase the margin between target and near-miss labels. Phase 2 refinement emerges from the interaction between loop-back retrieval and margin-widening writes (cf. Eq. 3). To distill this joint behavior, we match a pooled refinement score combining the pooled QK loop-back signal and pooled OV helpfulness. For $M \in \{T, S\}$ we define $\text{PRS}^M(q) = R^M(q) \cdot H^M(q)$, which mirrors the multiplicative structure of Eq. 3 at the pooled-head level. We minimize the teacher–student discrepancies in $R^M(q)$, $H^M(q)$, and $\text{PRS}^M(q)$ via the QK, OV, and interaction terms in Eq. 6.

Standard CoT Distillation

In Section 3 we include a standard chain-of-thought (CoT) distillation objective to transfer the teacher’s reasoning trace to the student. Following common practice in CoT distillation, training is performed under teacher forcing on the teacher-generated reasoning sequence. Concretely, for an input x , the teacher first produces a reasoning trace $\tau^T(x) = (t_1^T, \dots, t_m^T)$. Both teacher and student are then evaluated on the shared sequence $z^T(x) = [\text{prompt}(x); \tau^T(x)]$, allowing token-level distributions to be aligned at each position.

The CoT distillation loss combines cross-entropy on the teacher tokens with a KL divergence between the teacher and student output distributions:

$$\mathcal{L}_{\text{CoT}} = \mathbb{E}_x \sum_{t=1}^m \left[\underbrace{-\log p_S(t_t^T | z_{<t}^T)}_{\text{token supervision}} + \lambda_{\text{KL}} \underbrace{\text{KL}(p_T(\cdot | z_{<t}^T) \| p_S(\cdot | z_{<t}^T))}_{\text{distribution matching}} \right],$$

where p_T and p_S denote the teacher and student token distributions, respectively. This term provides the standard CoT supervision used in prior distillation work, while our proposed objectives focus on transferring the mechanistic behaviors of Phase 1 and Phase 2 reasoning.

C Dataset

MIMIC-IV-full. MIMIC-IV-full is derived from the MIMIC-IV electronic health record (EHR) dataset [Johnson et al., 2023], which contains deidentified ICU patient data from 2008–2019, including structured information and free-text clinical notes. In the clinical coding setting, instances correspond to discharge summaries annotated with ICD-10 codes, forming a high-dimensional multi-label prediction task. The dataset comprises 122,279 discharge summaries and 7,942 unique ICD-10 codes, exhibiting a long-tailed and highly sparse label distribution characteristic of real-world medical coding.

LF-WikiSeeAlso-320K. LF-WikiSeeAlso-320K is a large-scale extreme multi-label dataset constructed from Wikipedia, where each instance corresponds to an article and labels correspond to its “See Also” links, representing semantically related pages. It contains 1,779,881 training instances and 769,421 test instances with a label space of 501,070 unique labels. The dataset has an average of 4.75 labels per instance and 16.86 instances per label, reflecting moderate density alongside a long-tailed distribution. It models the task of related-article recommendation, requiring selection of a small subset of relevant labels from an extremely large candidate space, and has been used in recent work such as Dahiya et al. [2025]. The dataset is publicly available at <http://manikvarma.org/downloads/XC/XMLRepository.html>.

D Evaluation Metrics

D.1 CoT Fidelity Metric

Following Wang et al. [2023], our primary metric for teacher faithfulness is *Leakage-Adjusted Simulatability (LAS)*, which quantifies how well the student’s rationale helps a simulator recover the teacher’s (gold) answer. This measures the degree to which the student remains faithful to the teacher’s reasoning trace.

Formally, for a question q , student-generated rationale r , and the teacher’s gold answer a^* , teacher-faithfulness LAS is defined as

$$\text{LAS}_{\text{teacher}}(q, r, a^*) = \text{Acc}(q \oplus r \rightarrow a^*) - \text{Acc}(q \rightarrow a^*), \quad (8)$$

where \oplus denotes concatenation and Acc is the accuracy of a fine-tuned simulator model (typically T5-large) [Wang et al., 2023].

As complementary surface-level metrics of imitation, we report:

- Token-level alignment via BLEU-4 between the teacher trace \mathbf{c}^T and student trace \mathbf{c}^S [Ramesh et al., 2025]:

$$\text{BLEU}(\mathbf{c}^T, \mathbf{c}^S). \quad (9)$$

- Distributional alignment via perplexity of the teacher trace under the student model [Yan et al., 2025]:

$$\text{PPL}(\mathbf{c}^T | x) = \exp\left(\frac{1}{L} \sum_{t=1}^L -\log p_S(c_t^T | x, \mathbf{c}_{<t}^T)\right). \quad (10)$$

Higher teacher-faithfulness LAS, higher BLEU, and lower perplexity together indicate stronger faithfulness of the student toward the teacher’s reasoning trace.

D.2 Task-Specific Answer Accuracy

In addition to the fidelity metrics above, we extract the final answer a' from the student’s generated reasoning trace and evaluate it against the gold answer a^* using macro-F1. This metric measures the correctness of the final prediction, independent of trace-level imitation.

Let \mathcal{C} denote the set of classes. The macro-F1 score is

$$\text{Macro-F1} = \frac{1}{|\mathcal{C}|} \sum_{c \in \mathcal{C}} \text{F1}_c, \quad (11)$$

where

$$\text{F1}_c = \frac{2P_c R_c}{P_c + R_c}, \quad P_c = \frac{\text{TP}_c}{\text{TP}_c + \text{FP}_c}, \quad R_c = \frac{\text{TP}_c}{\text{TP}_c + \text{FN}_c},$$

and $\text{TP}_c, \text{FP}_c, \text{FN}_c$ are computed over binary predictions for class c in the multi-label setting.

E Statistical Significance

Statistical Significance via Wilcoxon Signed-Rank Test. We assess statistical significance using the non-parametric Wilcoxon Signed-Rank Test [Demšar, 2006] for comparing paired model outputs.

For metrics computed at the instance level (e.g., P@15), we apply the test directly to the paired per-instance scores between the base model and its PLANT-enhanced counterpart. For aggregate metrics such as F1 and AUC, which are reported as single values over the full test set, we first collect N paired scores—either from repeated evaluations (e.g., $N = 10$ in 10-fold cross-validation) or from N bootstrap resamples. Let $\{a_1, a_2, \dots, a_N\}$ and $\{b_1, b_2, \dots, b_N\}$ denote the scores of the base model and the PLANT-enhanced model, respectively. We compute the difference $d_i = b_i - a_i$ for each pair and rank the absolute values $|d_i|$ (excluding zeros), averaging ranks in the case of ties. Each rank is assigned the sign of d_i , and we compute the rank sums W^+ and W^- over positive and negative differences. The test statistic is $W = \min(W^+, W^-)$.

For small N , statistical significance is determined using exact Wilcoxon critical values; for larger N , we apply the normal approximation with

$$\mu = \frac{N(N+1)}{4}, \quad \sigma = \sqrt{\frac{N(N+1)(2N+1)}{24}},$$

$$z = \frac{W - \mu}{\sigma}.$$

We reject the null hypothesis of no difference if the resulting p -value is less than a threshold α (typically 0.05). In our tables, statistically significant improvements are marked using \blacktriangle . This test is readily implemented in standard libraries such as `scipy.stats.wilcoxon` in Python or `wilcox.test(paired=TRUE)` in R.

Reporting Gains with Confidence Intervals. We also report absolute gains along with 95% confidence intervals (CI) using paired bootstrap resampling. For each evaluation metric, we draw $B = 1000$ bootstrap samples from the test set and compute the difference $\Delta_b = \text{Metric}_b^{\text{PLANT}} - \text{Metric}_b^{\text{Base}}$ for each sample b . The reported gain is the mean $\hat{\mu}$ of $\{\Delta_b\}$, and the CI is computed using the percentile bootstrap method by taking the 2.5th and 97.5th percentiles of the empirical distribution of $\{\Delta_b\}$.

We mark results as statistically significant only if the Wilcoxon signed-rank test ($\alpha=0.05$) is passed *and* the 95% CI excludes 0. In such cases, we annotate the score with a colored arrow: \blacktriangle for statistically significant gains and \blacktriangledown for significant drops. If the CI includes 0, no arrow is shown. For example, 14.7 \blacktriangle (+1.2, [0.6, 1.8]) indicates a statistically significant gain over the base model, while 70.1 \blacktriangledown (-1.4, [-2.1, -0.7]) denotes a significant drop. In contrast, 73.8 (+0.3, [0.0, 0.6]) is not statistically significant and is shown without an arrow.

Note on Bootstrap Resampling. When N bootstrap resamples are used to obtain paired scores for the Wilcoxon signed-rank test, we note that the resamples are not strictly independent due to sampling with replacement. In such cases, we place primary emphasis on the bootstrap percentile confidence intervals for assessing the significance and magnitude of the difference; the Wilcoxon test is applied mainly for datasets where independent replicates (e.g., cross-validation folds) are available. Results are marked as statistically significant only when *both* the 95% CI excludes zero and the Wilcoxon test (where applicable) yields $p < 0.05$.

F Additional Results

In Table 2 we present the compressed results on the LF-WikiSeeAlso-320K dataset, combining both performance metrics and phase-specific mechanistic alignment scores for LLaMA3-7B and LLaMA3-13B students. See main paper Table 1 for the corresponding MIMIC-IV-full results.

In Table 3 we present additional distillation results using two different student backbones (QWEN3-4B and GEMMA-3-12B) from the same LLaMA3-70B teacher. See main paper Table 1 for results with LLaMA3-7B and LLaMA3-13B students.

In Table 4 we present additional results on phase specific mechanistic fidelity using two different student backbones (QWEN3-4B and GEMMA-3-12B) distilled from the same LLaMA3-70B teacher. See Table 1 for results with LLaMA3-7B and LLaMA3-13B students.

Table 2: **Mechanistic distillation improves reasoning quality and downstream performance on LF-WikiSeeAlso-320K.** See main paper Table 1 for MIMIC-IV-full results.

Model/Method	Focus \uparrow	Confusion \downarrow	LAS \uparrow	macro-F1 \uparrow	Sharpness \uparrow	AnchorAlign \uparrow	LoopBack \uparrow	Helpfulness \uparrow
LLaMA3-7B/Vanilla	0.41	0.32	0.71	0.47	1.84	0.42	0.31	0.28
LLaMA3-7B/Mech.	0.66* (+0.25)	0.16* (-0.16)	0.79* (+0.08)	0.57* (+0.10)	2.47* (+0.63)	0.61* (+0.19)	0.52* (+0.21)	0.46* (+0.18)
LLaMA3-13B/Vanilla	0.48	0.29	0.74	0.51	1.96	0.47	0.35	0.32
LLaMA3-13B/Mech.	0.70* (+0.22)	0.14* (-0.15)	0.81* (+0.07)	0.60* (+0.09)	2.55* (+0.59)	0.65* (+0.18)	0.56* (+0.21)	0.49* (+0.17)
Avg. gain with mech.	$\Delta+0.235$	$\nabla-0.155$	$\Delta+0.075$	$\Delta+0.095$	$\Delta+0.61$	$\Delta+0.19$	$\Delta+0.21$	$\Delta+0.18$
LLaMA3-70B/Teacher	0.75	0.12	0.85	0.67	2.71	0.72	0.63	0.58

Table 3: **Mechanistic distillation with different student backbones.** Results using Qwen3-4B and Gemma-3-12B as students. See main paper Table 1 for results with Llama students.

Model	Focus \uparrow	Confusion \downarrow	LAS \uparrow	macro-F1 \uparrow
Dataset: LF-WikiSeeAlso-320K				
QWEN3-4B (Vanilla)	0.36	0.37	0.66	0.41
QWEN3-4B (Mech)	0.60 \blacktriangle (+0.24)	0.18 \blacktriangledown (-0.19)	0.77 \blacktriangle (+0.11)	0.54 \blacktriangle (+0.13)
GEMMA-3-12B (Vanilla)	0.50	0.27	0.76	0.54
GEMMA-3-12B (Mech)	0.69 \blacktriangle (+0.19)	0.14 \blacktriangledown (-0.13)	0.82 \blacktriangle (+0.06)	0.62 \blacktriangle (+0.08)
Avg. gain with mech.	$\Delta+0.215$	$\nabla-0.16$	$\Delta+0.085$	$\Delta+0.105$
LLaMA3-70B (Teacher)	0.75	0.12	0.85	0.67
Dataset: MIMIC-IV-full				
QWEN3-4B (Vanilla)	0.34	0.39	0.64	0.39
QWEN3-4B (Mech)	0.58 \blacktriangle (+0.24)	0.20 \blacktriangledown (-0.19)	0.75 \blacktriangle (+0.11)	0.51 \blacktriangle (+0.12)
GEMMA-3-12B (Vanilla)	0.46	0.30	0.73	0.49
GEMMA-3-12B (Mech)	0.64 \blacktriangle (+0.18)	0.17 \blacktriangledown (-0.13)	0.79 \blacktriangle (+0.06)	0.57 \blacktriangle (+0.08)
Avg. gain with mech.	$\Delta+0.21$	$\nabla-0.16$	$\Delta+0.085$	$\Delta+0.10$
LLaMA3-70B (Teacher)	0.73	0.14	0.83	0.64

G Limitations

While our mechanistic characterization and distillation framework yields consistent improvements across datasets and model scales, several limitations remain.

Dependence on teacher quality. Our framework assumes that the teacher model exhibits strong and internally consistent reasoning behavior. If the teacher itself produces unstable or low-quality reasoning trajectories, the distilled student may inherit these deficiencies. Mechanistic supervision cannot compensate for fundamentally incorrect teacher reasoning.

Interpretability assumptions. Our characterization decomposes reasoning into two phases: coarse semantic focusing and later contrastive refinement. Although supported by multiple mechanistic analyses (e.g., activation patching, attention tracing, and temporal trajectory analysis), these phases remain an interpretive abstraction rather than a formally identifiable ground-truth decomposition of transformer computation. Different interpretability methodologies may yield alternative views of the same underlying mechanisms.

Restricted evaluation scope. We primarily evaluate reasoning over large label spaces in domains such as clinical coding and extreme multi-label retrieval. While these settings capture realistic “needle-in-a-haystack” reasoning scenarios, additional studies across broader reasoning tasks (e.g., mathematical reasoning, program synthesis, or multimodal reasoning) would further test the generality of the proposed mechanisms.

Computational overhead. Mechanistic analysis introduces additional computational cost beyond standard distillation, particularly for activation patching, head ranking, and phase-specific supervision.

Table 4: **Mechanistic distillation recovers phase-specific reasoning mechanisms with different student backbones.** Values are constituent sub-scores of CoarseScore (sharpness, anchor alignment) and RefineScore (QK loop-back, OV helpfulness) – see Eqs. 1 and 3. See main paper Table 1 for results with Llama students.

Model / Method	Sharpness \uparrow	Anchor align. \uparrow	QK loop-back \uparrow	OV helpfulness \uparrow
Dataset: LF-WikiSeeAlso-320K				
QWEN3-4B/ Vanilla	1.41	0.35	0.24	0.22
QWEN3-4B/ Mech.	2.12 \blacktriangle (+0.71)	0.54 \blacktriangle (+0.19)	0.44 \blacktriangle (+0.20)	0.39 \blacktriangle (+0.17)
GEMMA-3-12B/ Vanilla	1.92	0.46	0.34	0.31
GEMMA-3-12B/ Mech.	2.41 \blacktriangle (+0.49)	0.62 \blacktriangle (+0.16)	0.53 \blacktriangle (+0.19)	0.47 \blacktriangle (+0.16)
Avg. gain with mech.	Δ +0.60	Δ +0.175	Δ +0.195	Δ +0.165
LLaMA3-70B (Teacher)	2.71	0.72	0.63	0.58
Dataset: MIMIC-IV-full				
QWEN3-4B/ Vanilla	1.28	0.32	0.21	0.19
QWEN3-4B/ Mech.	1.92 \blacktriangle (+0.64)	0.49 \blacktriangle (+0.17)	0.39 \blacktriangle (+0.18)	0.35 \blacktriangle (+0.16)
GEMMA-3-12B/ Vanilla	1.68	0.41	0.29	0.26
GEMMA-3-12B/ Mech.	2.14 \blacktriangle (+0.46)	0.56 \blacktriangle (+0.15)	0.47 \blacktriangle (+0.18)	0.42 \blacktriangle (+0.16)
Avg. gain with mech.	Δ +0.55	Δ +0.16	Δ +0.18	Δ +0.16
LLaMA3-70B (Teacher)	2.45	0.65	0.57	0.52

Although these analyses are performed offline and do not affect inference efficiency, they increase overall experimentation cost during development.

Dependence on chain-of-thought supervision. Our method relies on access to teacher reasoning traces during distillation. In settings where high-quality reasoning traces are unavailable, restricted, or unreliable, the applicability of the proposed framework may be limited.

Open-weight model dependence. Our experiments are conducted using publicly available open-weight models. While this improves reproducibility and transparency, conclusions may not directly transfer to proprietary frontier systems whose internal architectures, training procedures, or decoding strategies are inaccessible.

H Broader Impacts

This work studies the mechanistic structure of reasoning in large language models and proposes a distillation framework that transfers these behaviors to smaller models. The research has both potentially beneficial and potentially harmful implications.

Positive impacts. Understanding how reasoning models operate over extremely large output spaces may improve the efficiency, interpretability, and accessibility of reasoning systems. Our framework enables smaller open models to better approximate the reasoning behavior of substantially larger systems, potentially reducing computational cost and increasing accessibility for researchers and practitioners with limited resources. Applications include large-scale retrieval, medical coding support, recommendation systems, and scientific information organization.

Additionally, mechanistic analyses may contribute to broader interpretability and alignment efforts by providing tools for understanding how reasoning trajectories evolve internally across transformer layers and heads.

Potential risks. Distilled reasoning systems could also be misused in high-stakes or safety-critical settings where incorrect outputs may appear deceptively well-reasoned. Because distilled models imitate reasoning behaviors from teachers, they may inherit systematic biases, hallucinations, or unsafe reasoning patterns present in the teacher model or training data.

Moreover, improvements in efficient reasoning over large candidate spaces could potentially be adapted for harmful applications such as large-scale surveillance, profiling, automated misinformation organization, or malicious retrieval systems.

Mitigations. To support responsible use, we rely exclusively on publicly available datasets and open-weight models released under their respective licenses. Our released artifacts are intended solely for research and reproducibility purposes. We encourage future work on mechanistic auditing, robustness analysis, and safety evaluation of distilled reasoning systems before deployment in high-stakes settings.